PNAS RESEARCH ARTICLE | MICROBIOLOGY

Antiactivators prevent self-sensing in *Pseudomonas aeruginosa* quorum sensing

Parker Smith[a] and Martin Schuster[a,1]

Edited by E. Greenberg, University of Washington, Seattle, WA; received January 27, 2022; accepted May 2, 2022

Quorum sensing is described as a widespread cell density-dependent signaling mechanism in bacteria. Groups of cells coordinate gene expression by secreting and responding to diffusible signal molecules. Theory, however, predicts that individual cells may short-circuit this mechanism by directly responding to the signals they produce irrespective of cell density. In this study, we characterize this self-sensing effect in the acyl-homoserine lactone quorum sensing system of *Pseudomonas aeruginosa*. We show that antiactivators, a set of proteins known to affect signal sensitivity, function to prevent self-sensing. Measuring quorum-sensing gene expression in individual cells at very low densities, we find that successive deletion of antiactivator genes *qteE* and *qslA* produces a bimodal response pattern, in which increasing proportions of constitutively induced cells coexist with uninduced cells. Comparing responses of signal-proficient and -deficient cells in cocultures, we find that signal-proficient cells show a much higher response in the antiactivator mutant background but not in the wild-type background. Our results experimentally demonstrate the antiactivator-dependent transition from group- to self-sensing in the quorum-sensing circuitry of *P. aeruginosa*. Taken together, these findings extend our understanding of the functional capacity of quorum sensing. They highlight the functional significance of antiactivators in the maintenance of group-level signaling and experimentally prove long-standing theoretical predictions.

quorum sensing | acyl-homoserine lactone | *Pseudomonas aeruginosa* | self-sensing | antiactivation

Significance

Canonical quorum sensing is characterized as a cell–cell communication process that bacteria use to coordinate group behaviors. Diffusible signal molecules induce gene expression in response to cell density. Here, we describe a mechanism in the acyl-homoserine lactone signaling pathway of *Pseudomonas aeruginosa* that ensures this sensing and response at the group level. We show that two accessory proteins termed antiactivators prevent self-sensing, the cell-autonomous and density-independent reception of signals produced by the same cell. Self-sensing in turn generates population-wide bimodality in gene expression that may explain the response heterogeneity observed in other quorum-sensing bacteria. The ability to experimentally tune the sensing mode adds functionality to the design of cell–cell signaling circuits in synthetic biology.

Bacterial quorum sensing (QS) is a widespread form of cell-to-cell signaling in which small, diffusible signaling molecules are secreted into the environment and sensed by a cognate cellular receptor (1, 2). Once bound to the signaling molecule, the receptor activates the transcription of target genes. The regulated gene products are involved in processes ranging from bioluminescence and virulence to biofilm formation and microbial warfare. Often, signal production is itself activated by QS, generating a positive feedback loop (3, 4). The general perception of QS in the literature is that this system coordinates the simultaneous activation of target genes at the group level once an extracellular threshold signal concentration (a "quorum") has been reached (1–7). Theoretical considerations suggest, however, that an alternative outcome is possible. Given appropriate network parameters, the signals could directly bind to the receptor in the same cell in which they are produced, by-passing an extracellular stage and essentially short-circuiting the system (8–12). This would lead to cell-autonomous, constitutive expression of target genes by some or all cells in the population, depending in part on the degree of cell-to-cell variability (11). Such "self-sensing" has been observed in the peptide-based QS system of the gram-positive bacterium *Bacillus subtilis*, although the underlying mechanism is not clear (13). Parameters that can influence self-sensing include the rates of intracellular signal synthesis and degradation, signal transport and diffusion out of the cell, and signal sensitivity of the cognate receptor (8–11, 13). In this study, we describe a self-sensing mechanism in the acyl-homoserine-lactone (AHL)-based QS system of the gram-negative bacterium *Pseudomonas aeruginosa*. The mechanism involves so-called antiactivator proteins that modulate signal sensitivity.

The opportunistic pathogen *P. aeruginosa* is a model organism for QS research with a well-understood AHL signaling circuit (6, 14). In *P. aeruginosa,* AHL signaling controls hundreds of genes that encode, for example, extracellular enzymes, toxins, and metabolites (5, 15). The primary AHL QS system in *P. aeruginosa* (termed *las*) is composed of the signal synthase LasI, which produces the AHL signal molecule 3-oxo-dodecanoyl-homoserine lactone (3OC12-HSL), and the receptor LasR. The diffusible 3OC12-HSL accumulates during growth, binds to LasR, and activates the expression of target genes, including *lasI* (16).

The sensitivity of the *P. aeruginosa* QS system to the 3OC12-HSL signal is determined by three nonhomologous antiactivator proteins (QteE, QslA, and QscR). Although functional details differ, they all sequester the LasR receptor, additively

Author affiliations: [a]Department of Microbiology, Oregon State University, Corvallis, OR 97331

Author contributions: P.S. and M.S. designed research; P.S. performed research; P.S. contributed new reagents/analytic tools; P.S. and M.S. analyzed data; P.S. and M.S. wrote the paper; and M.S. provided funding.

The authors declare no competing interest.

This article is a PNAS Direct Submission.

[1]To whom correspondence may be addressed. Email: martin.schuster@oregonstate.edu.

This article contains supporting information online at http://www.pnas.org/lookup/suppl/doi:10.1073/pnas.2201242119/-/DCSupplemental.

Published June 13, 2022.

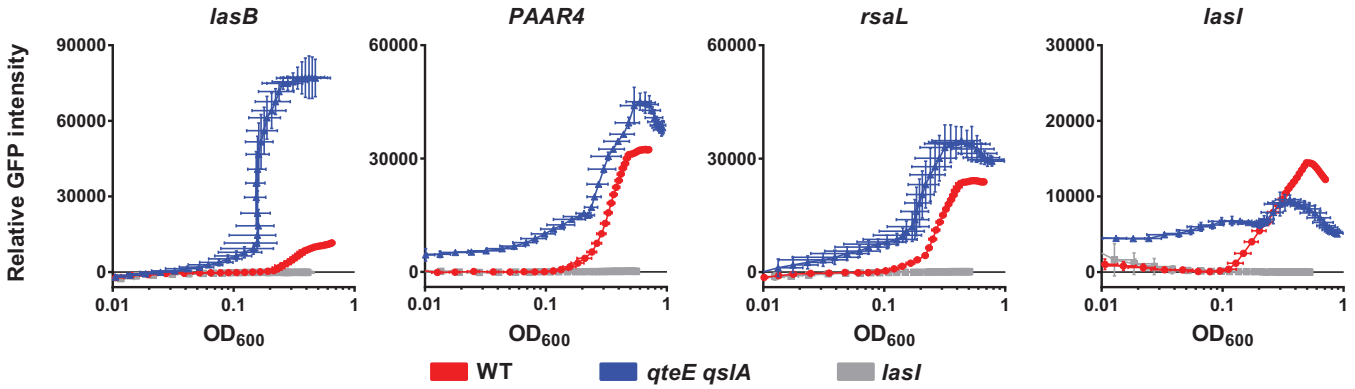

Fig. 1. Effect of antiactivation on QS-controlled genes. Cell density-dependent expression of *lasB′-gfp, PAAR4′-gfp, rsaL′-gfp,* and *lasI′-gfp* in the *P. aeruginosa* WT (red), the *qteE qslA* antiactivator double mutant (blue), and the *lasI* signal synthesis mutant (gray), grown in LB monoculture in a plate reader ($n = 3$). GFP fluorescence levels were normalized to cell density, expressed as OD_{600}.

reducing the induction threshold and delaying the activation of target genes (17–21). Antiactivation is not restricted to *P. aeruginosa*. The first-characterized antiactivator protein, TraM, attenuates QS-mediated plasmid transfer in the plant pathogen *Agrobacterium tumefaciens*, and TraM homologs are found in the *Rhizobiaceae* and *Bradyrhizobiaceae* families (12, 18, 22, 23).

In this study, we have explored the effects of different combinations of antiactivator deletions on the expression level and induction timing of LasR-3OC12-HSL–regulated genes in *P. aeruginosa*. We developed a cultivation and sampling approach in conjunction with flow cytometry to measure gene expression in single cells at very low cell densities. Using this approach, we were able to experimentally demonstrate a distinct function for antiactivators in *P. aeruginosa*. We found that antiactivators prevent self-sensing and are critical for maintaining group-level signaling.

Results

Effect of Antiactivators on the Expression of QS-Controlled Genes. In our previous study (17), we had examined the effect of combinations of *qslA*, *qteE*, and *qscR* antiactivator deletions on the expression of *lasB*, a well-characterized QS-controlled gene encoding the exoprotease elastase (24). We had found that antiactivator deletion results in earlier induction and higher expression levels, with double and triple deletions having a larger effect than single deletions. For the current study, we chose to focus on the *qteE qslA* mutant, because it was one of two mutants with the largest effect, and because it did not contain a deletion in *qscR*, which might complicate interpretation of results due to its hybrid role as activator and antiactivator (25). We further chose to investigate the role of antiactivation in the *las*-QS system, which is considered to be atop a QS regulatory hierarchy (6, 14, 26). We selected three well-characterized *las*-controlled target genes in addition to *lasB*. These are *lasI*, *rsaL*, and *PAAR4*, encoding the signal synthase of the *las* system, a repressor of *lasI* transcription, and a type VI secretion system effector protein, respectively (27–31). While *lasI*, *rsaL*, and *PAAR4* are solely controlled by the *las* system, *lasB* is also coregulated by another AHL QS system, termed *rhl* (RhlRI) (28).

We determined the expression of these genes as plasmid-borne promoter–green fluorescent protein (GFP) fusions. We measured bulk GFP fluorescence in the wild-type (WT) strain, the *qslA qteE* double mutant, and the *lasI* mutant grown in a standard rich medium (Lysogeny Broth, LB), inoculated from low-density cultures to minimize preexisting GFP expression. The expression of all four genes was at baseline levels in the *lasI* mutant control, demonstrating their tight regulation by the *las* system (Fig. 1). All genes, with the exception of *lasI*, were expressed at higher maximal levels in the *qteE qslA* mutant than in the WT, consistent with the effect of antiactivation on target gene expression. The attenuated expression of *lasI* in the *qteE qslA* mutant could be a consequence of the increased expression of *rsaL*, which in turn represses *lasI*. More importantly, all four genes were also induced at a lower cell density in the *qteE qslA* mutant than in the WT. In fact, *PAAR4* and *lasI* expression was substantially elevated at the lowest cell densities measured. It is possible that the expression of both genes is constitutive in the absence of antiactivation, potentially as a consequence of self-sensing.

Effect of Antiactivation on *lasI* Expression at the Single-Cell Level. To better characterize QS induction patterns at low cell density, we employed flow cytometry. This technique measures GFP expression at the single-cell level, offering several advantages over bulk fluorescence measurements. It can more precisely quantify gene expression and induction thresholds at very low densities, and it can reveal potential cell-to-cell heterogeneity in antiactivator-deficient QS gene expression.

To enable measurements at optical densities (optical density at 600 nm [OD_{600}]) much below 0.01, we devised two procedures. First, we developed a specific sampling protocol that entails the rapid concentration of large culture volumes by filtration and immediate fixation to preserve QS gene expression levels. Second, we implemented an extensive preculturing scheme to reduce GFP expression to background levels prior to experimental sampling (*SI Appendix*, Fig. S1). We chose the *lasI′-gfp* reporter for further flow-cytometric analysis, because it is a central QS component, it shows comparatively high induction in the antiactivator mutant at low cell density, and it is solely regulated by LasR-3OC12-HSL (28).

We quantified *lasI′-gfp* expression kinetics in the WT, the *qteE qslA* mutant, and the *lasI* mutant. We also included the *qteE* and *qslA* single mutants to assess the individual contributions of antiactivator proteins. Histograms of fluorescence intensity distributions illustrate how the population transitions from an off to an on state as culture density increases (Fig. 2*A*). Tight fluorescence peaks with near-normal distribution are apparent in the on state at high densities. However, the population distribution is very different at low cell densities. The *qslA qteE* mutant shows a bimodal distribution. A sizable proportion of cells is in the on state even at the lowest sampling density, potentially as a consequence of self-sensing. Generally, the proportion of cells in the

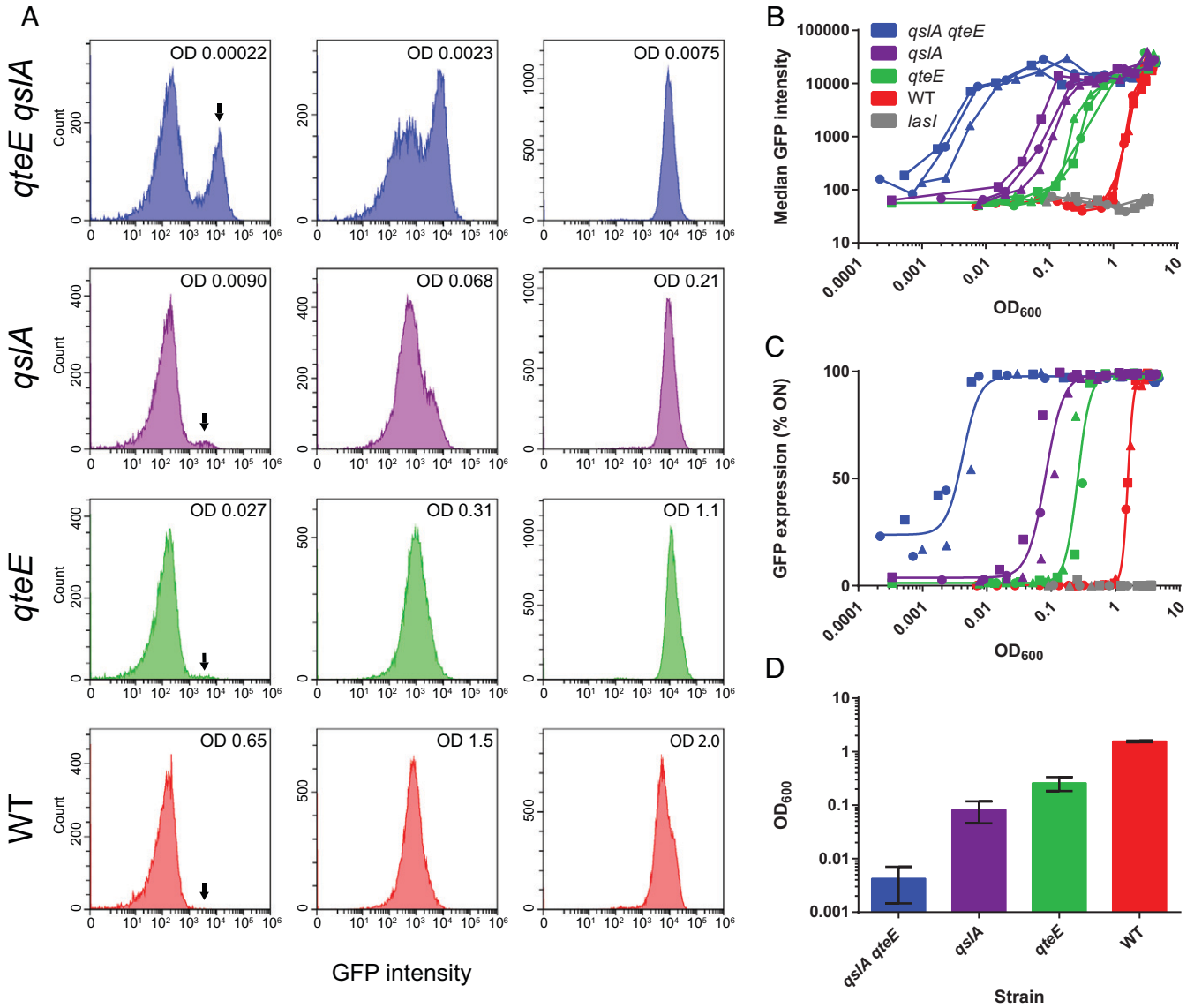

Fig. 2. Flow cytometry analysis of WT and antiactivator mutant cell populations carrying a *lasI′-gfp* reporter. (*A*) Selected histograms showing fluorescence distributions before, during, and after induction (left to right). The number on the top right indicates cell density (OD_{600}). The arrow indicates the subpopulation in the on state (from about a quarter in the *qslA qteE* mutant to absent in the WT). (*B*) Median GFP intensity of cell populations during the entire culturing period vs. cell density. Median values were determined from the respective histograms. Individual biological replicates are shown ($n = 3$). (*C*) Fraction of induced cells vs. cell density. Cells with a fluorescence intensity greater than 10^3 were considered to be ON. All replicate data were fit with a single curve, using a Hill-type sigmoidal function. The gray line in *B* and *C* indicates the *lasI* mutant baseline. (*D*) Cell-density values resulting in half-maximal *lasI* activation determined from a curve fit to the data in *C*. Error bars indicate SD. All values are significantly different from each other as determined by one-way ANOVA ($P < 0.05$).

on state, and hence the degree of heterogeneity, decreases in the order *qteE qslA* > *qslA* > *qteE* > WT.

A plot of median fluorescence data across the entire sampling range shows the activation kinetics of all strains. Loss of antiactivation resulted in progressively earlier activation, matching the order seen for the degree of heterogeneity in the histogram plots, and resulted in more gradual induction, contrasting the very rapid transition seen for the WT. A plot of the fraction of on cells, as determined by a fluorescence intensity threshold, vs. cell density (Fig. 2*C*) emphasizes the degree of heterogeneity observed at low cell density and revealed the cell densities at which half-maximal induction occurs (Fig. 2*D*). Taken together, our data are consistent with predictions made in a recent mathematical model of self- vs. group-sensing by Fujimoto and Sawai (11). This model predicts increasing cell–cell heterogeneity at the cellular level and a more gradual transition at the population level as the QS mode shifts from group-sensing to self-sensing (see *Discussion* for more details).

Signal Sensitivity of *lasI*-Deficient Antiactivator Mutants. Having demonstrated the cell density-dependent expression of *lasI′-gfp* in the different antiactivator mutants, we sought to determine the corresponding acyl-HSL concentrations necessary for activation. Toward this goal, we generated *lasI* deletions in our suite of antiactivator mutants and introduced the *lasI′-gfp* reporter plasmid. We then cultivated the resulting strains in the presence of various concentrations of synthetic 3OC12-HSL and measured bulk GFP fluorescence with a plate reader. We obtained dose–response curves that illustrate the large differences in signal sensitivity between the strains, spanning two orders of magnitude (Fig. 3). The order of the signal concentrations necessary for half-maximal activation correlates with the

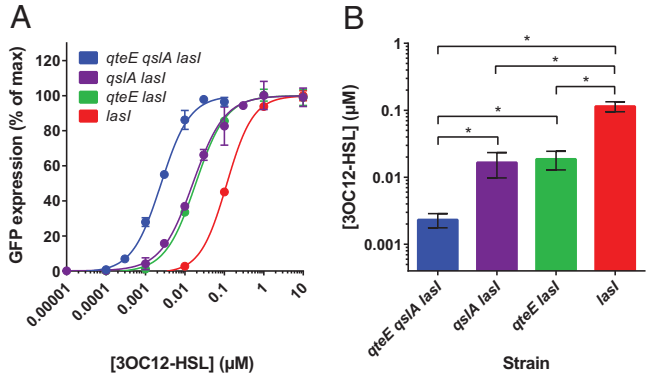

Fig. 3. AHL sensitivity of antiactivator mutants. (*A*) Relative GFP expression as a function of 3OC12-HSL concentration. Signal synthesis mutants were grown to saturation with increasing concentrations of exogenous, synthetic 3OC12-HSL signal ($n = 3$). The expression of the *lasI′-gfp* reporter construct in these strains was measured using a fluorescence plate reader. The data were fit with a Hill-type sigmoidal curve to determine the half-maximal induction of each strain. (*B*) Signal concentrations resulting in half-maximal induction. Error bars indicate SD. With one exception, all pairwise comparisons are significantly different from each other as determined by one-way ANOVA (*$P < 0.05$).

order of the cell densities in Fig. 2. In all cases, GFP expression was strictly dependent on added 3OC12-HSL.

Proof of Self-Sensing in the Antiactivator Double Mutant. Our flow cytometry experiments in Fig. 2 revealed the largest level of gene expression heterogeneity in *qteE qslA* double-mutant populations, with the highest proportion of cells in the on state at the lowest cell density sampled. We hypothesized that these cells are induced as a consequence of self-sensing. To test this hypothesis directly, we designed a coculturing scheme in which we combined *lasI*-proficient and *lasI*-deficient strains (herein abbreviated as I^+ and I^-, respectively) and measured *lasI′-gfp* expression in each strain by flow cytometry (Fig. 4*A*). The *qteE qslA* mutant and the *qteE qslA lasI* mutant formed the experimental strain pair (Q^-), while the WT and the *lasI* mutant formed the control strain pair (Q^+). The respective I^- cells served as "biosensors" that only respond to the 3OC12-HSL released by I^+ cells. This setup allowed us to distinguish self-sensing from group-sensing. In self-sensing, gene expression is expected to be substantially higher in I^+ than in I^- cells, because induction is governed by the feedback from intracellular signal that accumulates in individual I^+ cells. In contrast, in group-sensing gene expression is expected to be very similar in I^+ and in I^- cells, because activation is driven by feedback from the accumulation of shared, extracellular signal. Theory predicts that the contribution from intracellular signal synthesis (even if signal does not accumulate and quickly diffuses out of the cell) will always cause at least slightly higher QS activity in the I^+ than in the I^- strain (32). However, this contribution is expected to be very small in group-sensing compared with self-sensing.

To differentiate I^+ and I^- cells in coculture, we reciprocally labeled them with distinct fluorescent probes, DsRed-Express2 and E2Crimson. The tags were alternated between strains in each pair to address possible differences in their effects on gene expression, although we minimized this effect through fluorescence compensation in the flow cytometry software (*SI Appendix*, Fig. S2*A*). We further verified that cells harboring either tag in mixed culture can be clearly distinguished by flow cytometry (*SI Appendix*, Fig. S2*B*). We employed essentially the same growth conditions and precultivation scheme as described for the single-culture experiments described above. However, we added another preculture step before mixing strains together. We grew individual cultures of I^- strains with added signal alongside the respective I^+ strains without added signal. This step ensured that both I^+ and I^- strains started out with the same initial GFP expression levels, such that subsequent differences in experimental samples could be solely attributed to distinct QS modes rather than preculture histories. In preceding experiments, we had determined the appropriate concentrations of synthetic 3OC12-HSL that restore *lasI′-gfp* expression to WT levels (*SI Appendix*, Fig. S3).

The analysis of GFP expression data revealed striking differences between the Q^+ and Q^- cocultures, which are particularly apparent in the histograms of fluorescence intensity distributions (Fig. 4*B*). In the Q^- cocultures, the I^+ cells were partially induced at the lowest densities sampled, consistent with the single culture results above (Fig. 2*A*), whereas the I^- cells were not. The I^- cells showed increased expression during continued growth but always remained below the I^+ cells. In contrast, in the Q^+ cocultures both cell types were initially fully in the off state and then shifted to the on state simultaneously as the population density increased (Fig. 4*B*). Graphs of the median fluorescence of the populations vs. the cell density of the I^+ strain in each pair reflect these trends over the entire sampling range (Fig. 4*C*). To quantify the differences in expression kinetics between I^+ and I^- strains, we graphed the response ratio for each strain pair against the cell density and against the median GFP intensity of the respective I^+ strain (Fig. 4 *D* and *E*). Both graphs illustrate the much higher response ratios in the Q^- strain pair compared with the Q^+ strain pair. In fact, the response ratios for the Q^+ strain pair were very close to 1. In the Q^- coculture, the highest response ratios were achieved at low cell densities. This is consistent with a self-sensing model, where in the absence of antiactivators induction is driven by intracellular signal feedback in I^+ strains at low cell densities, before the accumulation of extracellular signal also contributes to induction in I^- strains at higher cell densities. Statistical analysis shows that these preinduction response ratios are significantly different between strain pairs and that they are also significantly above 1 in both cases (Fig. 4*F*), supporting our predictions.

Discussion

In this study, we have experimentally described self-sensing in a QS bacterial population, and we have characterized antiactivation as a governing mechanism that prevents it. We employed the well-understood AHL signaling system of the opportunistic pathogen *P. aeruginosa* as our experimental model. Self-sensing has been shown in the peptide-based QS system of *B. subtilis*, although the mechanism is not fully understood (13). Peptide signals are secreted into the environment and then sensed by a membrane receptor (33). How the signal producer gains preferential access to the signal in this system is unclear. In acyl-HSL signaling systems, the signals are produced intracellularly and generally freely diffuse across the cell envelope, although active transport is sometimes involved (4). The AHL signal is sensed intracellularly by a cytoplasmic receptor and transcriptional regulator, such that the potential for self-sensing is evident. Of note, the concept of "diffusion sensing," in which an individual cell would perceive self-produced QS signals that accumulate in a confined extracellular space, is not considered self-sensing in this context (34).

The *P. aeruginosa* acyl-HSL QS circuitry contains three antiactivator proteins that sequester the QS receptor LasR, thereby

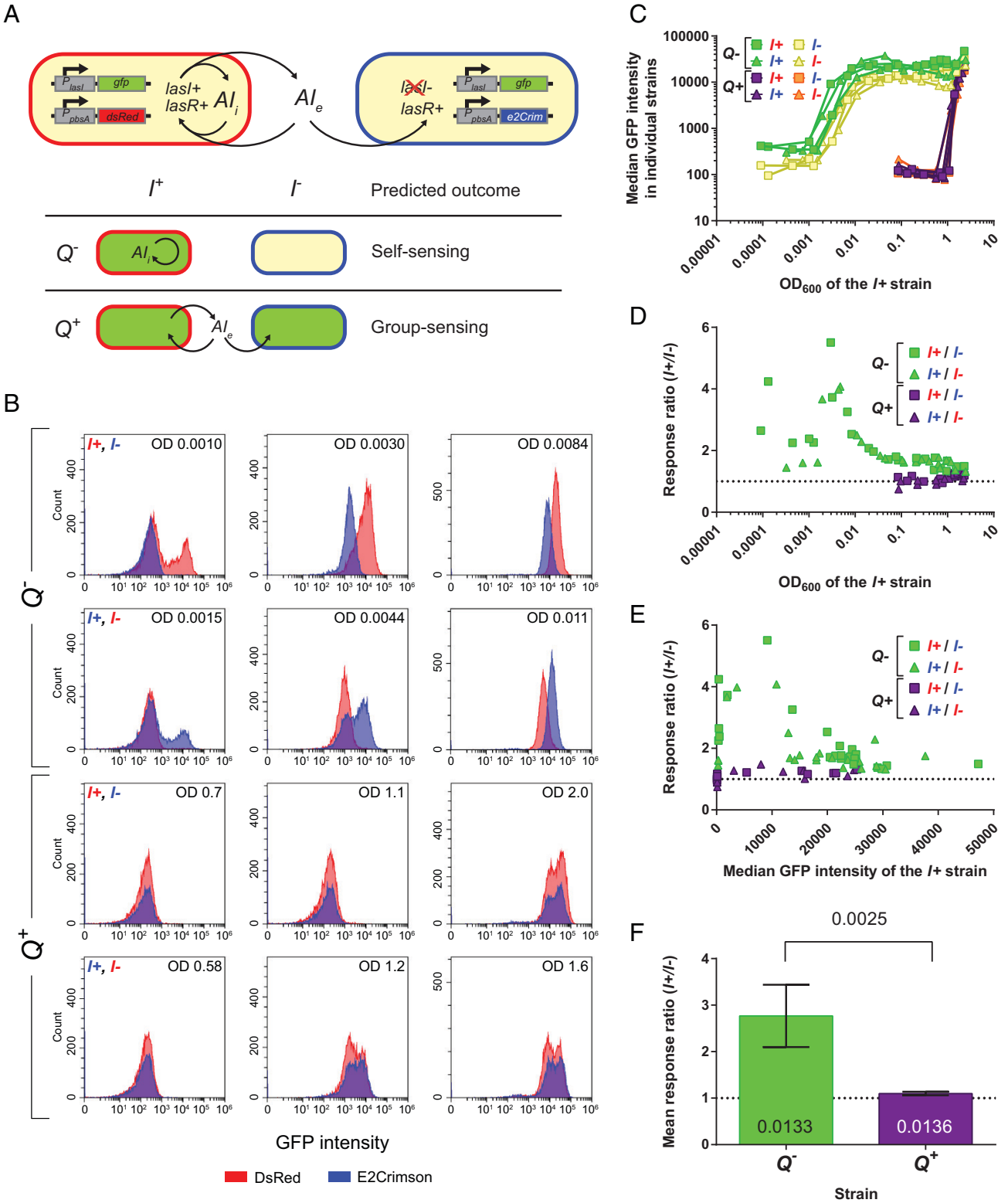

Fig. 4. Antiactivator-dependent self-sensing in cocultures of signal producers and nonproducers. Individual *P. aeruginosa* strains carrying the *lasI'-gfp* reporter in cocultures are denoted as follows: Q^+, antiactivator (*qslA qteE*)-proficient; Q^-, antiactivator (*qslA qteE*)-deficient; I^+, signal (*lasI*)-proficient; I^-, signal (*lasI*)-deficient. (*A*) Diagram of experimental coculture design with expected outcomes. Only one of two possible red-tag combinations is shown. (*B*) Selected histograms showing the fluorescence distributions of the I^+ and I^- subpopulations in cocultures before, during, and after induction (left to right). The number on the top right indicates cell density (OD_{600}). The subpopulation labeled with E2-Crimson is represented by blue histograms and the subpopulation labeled with DsRed-Express2 is represented by red histograms. (*C*) Median GFP intensity of subpopulations during the culturing period vs. the cell density of the I^+ strain ($n = 4$; two for each of the two red-tag combinations). (*D*) Response ratios vs. the cell density of the I^+ strain. (*E*) Response ratios vs. the median GFP intensity of the I^+ strain. In *C*–*E*, reciprocal labeling of I^+ and I^- cells by the respective red tags is indicated by squares vs. triangles. (*F*) Mean presaturation response ratios of the Q^+ and Q^- strain pairs. This mean response ratio was determined by averaging the individual response ratios of all samples for which the median GFP intensity of the I^+ strain was below 20,000. Error bars represent SD of the mean. *P* values were calculated using a one-sample Student's *t* test to determine significant difference from 1 and using a two-sample Student's *t* test to determine significant difference between two samples. The superscripts $^+$ and $^-$ for both *Q* and *I* genes were changed to + and – for small font sizes to improve legibility.

increasing the signal threshold necessary for induction. In our study, we focused on two antiactivators, QteE and QslA, that we previously found to exert the largest effect on QS gene expression (17). QteE reduces LasR protein stability, likely through direct protein–protein interaction (21). QslA in turn binds LasR to disrupt its dimerization and subsequent DNA binding but does not appear to reduce LasR protein stability (19). Moreover, *qteE* is activated by acyl-HSL QS, permitting negative feedback control (28).

Using *gfp* reporter fusions, we initially measured the expression of four QS-controlled genes in the WT and the *qteE qslA* double mutant at the population level (Fig. 1). We found that these genes respond differently to the lack of antiactivation. The reasons for this are not entirely clear and likely involve multiple factors during transcription initiation at target promoters, besides LasR binding affinity alone (27). As mentioned above, these factors include activation by the second acyl-HSL system (*rhl*) in the case of *lasB* (28) and negative feedback regulation by RsaL in the case of *lasI* (29, 35).

Next, we quantified the expression of *lasI'-gfp* in antiactivator single and double mutants at the single-cell level. To enable measurements at very low cell densities, we implemented a sampling procedure that concentrated large volumes of culture and a cultivation scheme that reduced preexisting GFP expression to background levels. Our flow cytometry data showed that successive deletion of antiactivators greatly reduces the induction threshold (with approximately 10-fold reduction in the *qteE* and *qslA* single mutants and approximately 100-fold reduction in the *qteE qslA* double mutant) and increases the proportion of constitutively active cells (Figs. 2 and 3). Despite apparent mechanistic differences, *qteE* and *qslA* single mutants both showed similar QS responses. To prove that the observed patterns are caused by antiactivator-dependent self-sensing, we designed a cocultivation procedure of signal-proficient and -deficient cells distinguishable by different red fluorescent tags. While the antiactivator-proficient strain pair showed a near-simultaneous response, the antiactivator-deficient strain pair showed a substantial difference: Signal-proficient cells showed a much higher and earlier response than signal-deficient cells (Fig. 4).

Self-sensing has been proposed in several theoretical studies (8–12). If network parameters are such that the intracellular signal concentration exceeds the induction threshold, self-sensing occurs. One modeling study in particular investigated the transition between group-sensing and self-sensing in QS populations (11). Fujimoto and Sawai showed that cell-to-cell variability in gene expression can lead to heterogeneous populations in which some cells self-activate and others do not, if the intracellular signal concentrations are near the induction threshold. They further predicted that the proportion of self-activating cells gradually increases with cell density as the accumulation of extracellular signal contributes to activation. The similarities to our experimental results are striking (although their modeling results were obtained at steady state, whereas our gene expression measurements were obtained in dynamic batch culture). Our flow cytometry data show a heterogeneous, bimodal induction pattern for the antiactivator double mutant, with a rather gradual increase in the proportion of induced cells, in contrast to the unimodal and rapid induction pattern for the WT (Fig. 2). Bimodality can emerge from a bistable QS system, which is what Fujimoto and Sawai assumed for their model, and which is plausible for the *las* system of *P. aeruginosa* (10, 32).

Intriguingly, heterogeneity in QS gene expression has recently been observed in several other bacterial species (7, 36–40). While the underlying mechanisms are not clear, our work suggests that self-sensing may be involved. These observations also indicate that self-sensing is physiologically relevant. The emergent phenotypic diversity at the population level offers potential benefits, including bet-hedging in dynamic environments, or a division of labor in biofilm communities (41, 42). Likewise, group-to self-sensing transitions may be relevant to the physiology of *P. aeruginosa* itself. There may be environmental conditions, for example nutrient stress, that promote self-sensing by enhancing signal production or lowering the induction threshold (43). Regulation may be at the level of LasI, LasR, or any of the antiactivator proteins. These mechanisms may also lead to a scenario where all cells in the population "self-sense," which we did not observe here but which would occur if the intracellular signal concentration was significantly above the induction threshold. Other components that could contribute to limiting self-sensing include the third antiactivator, QscR, the transcriptional repressor, RsaL, or an as-yet-uncharacterized, fourth antiactivator.

Our work suggests a function—in an evolutionary sense—for antiactivators in QS systems. Antiactivators not only tune the QS induction threshold but they also enable canonical group-sensing by suppressing self-sensing. From this perspective, it may become clearer why *P. aeruginosa* harbors three, rather than just one, antiactivator protein. All three might provide a partially redundant "fail-safe" mechanism to ensure group-level QS. Other, not necessarily mutually exclusive, functions are plausible. For example, the acquisition of one or multiple antiactivators could result in a "cheater" phenotype (44). These cells would exploit neighboring cells with no or fewer antiactivators that express QS-controlled secretions at a higher level. In certain contexts, antiactivation might be preferred over other mechanisms that could provide the same effect, such as a decrease in the affinity of the receptor to its signal, which in turn would be accompanied by a loss in signal specificity (45). Nevertheless, it is evident that not all QS systems require antiactivation to enable group-level signaling.

The antiactivators thus far identified and characterized are QteE, QslA, and QscR in *P. aeruginosa*, as well as TraM and TrlR (TraS) in *A. tumefaciens* (12, 22, 46). In some strains of *A. tumefaciens*, two TraM-type antiactivators function in parallel QS systems (47, 48). QscR and TrlR are LuxR homologs, whereas the other antiactivator proteins are unique, without any sequence similarity to each other. TraM homologs are found in Rhizobiaceae and Bradyrhizobiaceae (18). The structural and mechanistic diversity of antiactivators allows for different functional roles and suggests that novel antiactivator proteins remain to be discovered in other QS systems and species as well. Regardless of its prevalence, antiactivation has provided us with a tool to investigate the balance between self- and group-sensing in a QS population. This knowledge is of fundamental importance to our understanding of the functional capacity of QS systems and may find application in synthetic biology to design QS circuits with specific properties.

Materials and Methods

Strains, Plasmids, and Growth Conditions. All strains and plasmids used in this study are listed in *SI Appendix*, Table S1. *P. aeruginosa* PAO1 (Iglewski lineage) was used as the WT strain (49). All other strains, including antiactivator and signal synthesis mutants, are derived from this PAO1 parent. Plasmid pPROBE-AT harbors all QS-responsive *gfp* promoter fusions, expressing the stable and fast-folding GFP variant *gfpmut1* (50). Compatible plasmids pSW002-P_{psbA}-DsRed-Express2 and pSW002-P_{psbA}-E2-Crimson carry constitutively expressed DsRed-Express2 and E2-Crimson, respectively (51). These two fluorescent proteins are tetrameric, nontoxic, and derived from the same precursor protein. They have distinct emission peaks in the near red and far red, respectively. All plasmids are low to medium

copy number and highly stable (50, 51). The promoter-probe vector pPROBE-AT contains the tightly controlled pBBR1 replicon, which ensures high copy number stability over time (50, 52), as well as low within-population heterogeneity of unimodal distribution (7, 52, 53) similar to that in chromosomal constructs (53).

All routine and experimental cultures were grown at 37 °C on Lennox LB agar or with shaking at 250 rpm in Lennox LB medium buffered with 50 mM 3-(*N*-morpholino)-propanesulfonic acid (MOPS), pH 7.0. As a general preculturing scheme for all experimental assays, colonies were picked from plates, suspended in LB-MOPS medium, and inoculated at an initial OD_{600} of 0.001 in 3 to 5 mL LB-MOPS medium. Liquid cultures were grown to the indicated times and cell densities for subsequent cultivation. For plasmid maintenance and selection, the following antibiotic concentrations were used: For *P. aeruginosa,* 200 μg/mL carbenicillin and 80 μg/mL tetracycline, and for *Escherichia coli*, 10 μg/mL tetracycline. Synthetic 3OC12-HSL (RTI International) was dissolved in acidified ethyl acetate and dried on the bottom of culture tubes prior to the addition of culture medium.

Strain Construction. Plasmids were introduced into *P. aeruginosa* strains by transformation of chemically competent cells (54). A markerless, chromosomal deletion of *lasI* in antiactivator mutants was constructed by introducing the previously constructed pEX18Tc.Δ*lasI* suicide vector (55) into *qslA, qteE,* and *qslA qteE* mutant strains using standard gene replacement protocols (56). To construct *lasI′-gfp*, *rsaL′-gfp*, and *PAAR4′-gfp* transcriptional fusions, the respective promoter regions were PCR-amplified from the PAO1 genome using the following primers: *lasI*, forward primer 5′-NNNNNNAAGCTTACTGCCGCAGGATTGGCTTAT-3′ and reverse primer 5′-NNNNNNGAATTCCTCCAAATAGGAAGCTGAAGAATTTATG CAAA-3′; *rsaL*, forward primer 5′-NNNNNNAAGCTTGAAGAATTTATGCAAATTTCATAA-3′ and reverse primer 5′-NNNNNNGAATTCTCTTTTCGGACGTTTCTTCG-3′; *PAAR4*, forward primer 5′-NNNNNNAAGCTTCGGTCTCGCGCAGGGC-3′ and reverse primer 5′-NNNNNNGAATTCCCTGGCACTCTGCCGTGC-3′. Each PCR product was digested with HindIII and EcoRI (restriction sites underlined) and ligated with the equally digested promoter probe vector pProbe-AT (50). The resulting constructs were confirmed by sequencing.

Measurement of Bulk Fluorescence. For measurements of bulk fluorescence over time, experimental cultures were inoculated from precultures grown to an OD_{600} of 0.05 to 0.2. Three replicates of each culture were inoculated in 200 μL of LB medium in black-walled 96-well plates (655090; Greiner Bio-One), to an initial OD_{600} of 0.001. The cultures were grown uncovered, in a Tecan Infinite M200 multifunction plate reader with shaking at 37 °C. OD_{600} and fluorescence measurements (GFP, $\lambda_{excitation} = 480$ nm, $\lambda_{emission} = 535$ nm) were taken every 12 min. Relative fluorescence units were obtained by dividing the total fluorescence by the corresponding OD_{600}. The *gfp* reporter activity for individual strains was corrected for background fluorescence by subtracting the relative fluorescence of a control strain carrying the empty pProbe-AT plasmid.

To quantify the response of *lasI* strains to exogenous 3OC12-HSL, experimental cultures were again inoculated from precultures to an initial OD_{600} of 0.001, in 10 to 15 mL of LB-MOPS medium. After 3 h, 500-μL aliquots were transferred to a 96-well deep-well block with the appropriate concentrations of synthetic 3OC12-HSL dried down in the wells. After another 9 h of growth in the deep-well block, 200-μL aliquots were transferred to a black-walled 96-well plate. GFP fluorescence and OD_{600} were measured, and relative fluorescence units were calculated as described above. Relative fluorescence from this single time-point assay was graphed as a function of 3OC12-HSL concentration. The signal concentration at which half-maximal induction is achieved was determined by fitting a Hill-type sigmoidal function (Graphpad Prism).

Measurement of Single-Cell Fluorescence by Flow Cytometry. Flow cytometry was used to measure gene expression at the single-cell level. For pure culture experiments, 100 to 125 mL of LB-MOPS medium in 500-mL baffled flasks were inoculated from precultures grown to an OD_{600} of 0.1 to 0.2. Preculture aliquots were first diluted to an OD_{600} 0.01 and then further serially diluted 10,000-fold to give an initial OD_{600} of 10^{-7}. This scheme diluted cellular GFP to background levels through multiple rounds of cell division. For coculture experiments, individually grown preculture aliquots were combined at a 50:50 ratio and diluted to produce the same initial OD_{600} of 10^{-7}. For those coculture experiments involving *lasI* mutant biosensor strains, the precultivation scheme was modified. Individual precultures were initiated as described above and grown for 12 h total. However, after 3 h, synthetic 3OC12-HSL was added to the *lasI* mutant cultures (at final concentrations of 10 μM for the *lasI* single mutant and 0.1 μM for the *qslA qteE lasI* triple mutant). This step was taken to induce *lasI′-gfp* expression in the *lasI* mutant strains to levels identical to those in the respective *lasI*$^+$ strains (*SI Appendix*, Fig. S3). Individual precultures were now mixed as a 50:50 coculture of the respective *lasI*$^+$/*lasI*$^-$ strain pair. A second preculture was inoculated with this mixture to an initial OD_{600} of 0.001, grown to an OD_{600} of 0.1 to 0.2, and again used to inoculate an experimental coculture to an initial OD_{600} of 10^{-7}, in principle as described above.

Samples were taken regularly from all experimental cultures throughout growth, from exponential to stationary phase. Cell density was measured as OD_{600} using a spectrophotometer (Eppendorf Biophotometer). Cells were immediately concentrated and fixed for flow cytometry. Low-density samples (5 to 20 mL) were filter-concentrated using Vivaspin 500 filters with a 0.2-μm polyethersulfone membrane (Sartorius) connected to a vacuum pump. Higher-density samples were pelleted by centrifugation. Concentrated cells were resuspended in 200 μL phosphate-buffered saline (PBS), pH 7.2, fixed immediately by adding 4% paraformaldehyde to a final concentration of 2.5% (wt/vol), and gently shaken for 10 min at room temperature. Fixation followed a previously established protocol that fully preserves GFP fluorescence in *P. aeruginosa* (7). Cells were then washed twice and stored in PBS at 4 °C, with the cell density adjusted to an OD_{600} of 0.01.

Cell fluorescence was quantified using a Beckman-Coulter CytoFLEX S flow cytometer. The emission filters used were FITC 525/40 nm for GFP, PE 585/42 nm for dsRed Express, and APC 660/10 nm for E2Crimson. A manual threshold of 8,000 was set in the forward scatter height channel, and 20,000 instances were recorded for each sample. Cells expressing either DsRed-Express or E2Crimson were distinguished by gating using scatter plots of APC-area vs. PE-area. Data were analyzed with the Cytoexpert software. Minimal spectral bleed-through from the red channels into the GFP channel was removed using the gain-independent compensation function in the software. Fluorescence data are presented in raw form as histograms, as population median over cell density, and as percentage of the population in the on state over cell density. The fluorescence threshold that defines cells in the on state was 1×10^3. The "percent-on" data were fit using a Hill-type sigmoidal function (Graphpad Prism) to determine the density at which 50% of the cells are induced. For cocultures, a response ratio was determined using the equation $\frac{\text{GFP intensity } lasI^+}{\text{GFP intensity } lasI^-}$.

Statistical Analysis. Statistical analysis of experimental data was performed using GraphPad Prism (version 6.00 for Windows; GraphPad Software). The specific statistical test used is described in the respective figure legend. A one-way ANOVA was always paired with a multiple comparison analysis, comparing individual samples as indicated. Tukey's multiple comparison test was used to compare each condition to each other condition in Figs. 2*D* and 3*B*, and Dunnet's multiple comparison test was used to compare each experimental condition to a control in *SI Appendix*, Figs. S1 and S3.

Data Availability. All study data are included in the article and/or *SI Appendix*.

ACKNOWLEDGMENTS. We thank Rashmi Gupta and Cara Wilder for their gifts of previously constructed plasmids. We thank Malcolm Lowry, Allison Ehrlich, and the Kolluri lab for their assistance with flow cytometry. This study was funded by NSF grant MCB2106212 to M.S.

1. C. M. Waters, B. L. Bassler, Quorum sensing: Cell-to-cell communication in bacteria. *Annu. Rev. Cell Dev. Biol.* **21**, 319–346 (2005).
2. K. L. Asfahl, M. Schuster, Social interactions in bacterial cell-cell signaling. *FEMS Microbiol. Rev.* **41**, 92–107 (2017).
3. R. Popat, D. M. Cornforth, L. McNally, S. P. Brown, Collective sensing and collective responses in quorum-sensing bacteria. *J. R. Soc. Interface* **12**, 20140882 (2015).
4. K. Papenfort, B. L. Bassler, Quorum sensing signal-response systems in Gram-negative bacteria. *Nat. Rev. Microbiol.* **14**, 576–588 (2016).
5. M. Schuster, D. J. Sexton, S. P. Diggle, E. P. Greenberg, Acyl-homoserine lactone quorum sensing: From evolution to application. *Annu. Rev. Microbiol.* **67**, 43–63 (2013).
6. P. Williams, M. Cámara, Quorum sensing and environmental adaptation in *Pseudomonas aeruginosa*: A tale of regulatory networks and multifunctional signal molecules. *Curr. Opin. Microbiol.* **12**, 182–191 (2009).
7. R. L. Scholz, E. P. Greenberg, Positive autoregulation of an acyl-homoserine lactone quorum-sensing circuit synchronizes the population response. *MBio* **8**, e01079-17 (2017).
8. A. Pai, L. You, Optimal tuning of bacterial sensing potential. *Mol. Syst. Biol.* **5**, 286 (2009).

9. A. B. Goryachev *et al.*, Transition to quorum sensing in an *Agrobacterium population*: A stochastic model. *PLOS Comput. Biol.* **1**, e37 (2005).
10. A. B. Goryachev, Understanding bacterial cell-cell communication with computational modeling. *Chem. Rev.* **111**, 238–250 (2011).
11. K. Fujimoto, S. Sawai, A design principle of group-level decision making in cell populations. *PLOS Comput. Biol.* **9**, e1003110 (2013).
12. C. Fuqua, M. Burbea, S. C. Winans, Activity of the *Agrobacterium* Ti plasmid conjugal transfer regulator TraR is inhibited by the product of the *traM* gene. *J. Bacteriol.* **177**, 1367–1373 (1995).
13. T. Bareia, S. Pollak, A. Eldar, Self-sensing in *Bacillus subtilis* quorum-sensing systems. *Nat. Microbiol.* **3**, 83–89 (2018).
14. M. Schuster, E. P. Greenberg, A network of networks: Quorum-sensing gene regulation in *Pseudomonas aeruginosa*. *Int. J. Med. Microbiol.* **296**, 73–81 (2006).
15. V. E. Wagner, D. Bushnell, L. Passador, A. I. Brooks, B. H. Iglewski, Microarray analysis of *Pseudomonas aeruginosa* quorum-sensing regulons: Effects of growth phase and environment. *J. Bacteriol.* **185**, 2080–2095 (2003).
16. P. C. Seed, L. Passador, B. H. Iglewski, Activation of the *Pseudomonas aeruginosa lasI* gene by LasR and the *Pseudomonas* autoinducer PAI: An autoinduction regulatory hierarchy. *J. Bacteriol.* **177**, 654–659 (1995).
17. K. L. Asfahl, M. Schuster, Additive effects of quorum sensing anti-activators on *Pseudomonas aeruginosa* virulence traits and transcriptome. *Front. Microbiol.* **8**, 2654 (2018).
18. G. Chen, P. D. Jeffrey, C. Fuqua, Y. Shi, L. Chen, Structural basis for antiactivation in bacterial quorum sensing. *Proc. Natl. Acad. Sci. U.S.A.* **104**, 16474–16479 (2007).
19. H. Fan *et al.*, QslA disrupts LasR dimerization in antiactivation of bacterial quorum sensing. *Proc. Natl. Acad. Sci. U.S.A.* **110**, 20765–20770 (2013).
20. F. Ledgham *et al.*, Interactions of the quorum sensing regulator QscR: Interaction with itself and the other regulators of *Pseudomonas aeruginosa* LasR and RhlR. *Mol. Microbiol.* **48**, 199–210 (2003).
21. R. Siehnel *et al.*, A unique regulator controls the activation threshold of quorum-regulated genes in *Pseudomonas aeruginosa*. *Proc. Natl. Acad. Sci. U.S.A.* **107**, 7916–7921 (2010).
22. I. Hwang, D. M. Cook, S. K. Farrand, A new regulatory element modulates homoserine lactone-mediated autoinduction of Ti plasmid conjugal transfer. *J. Bacteriol.* **177**, 449–458 (1995).
23. K. R. Piper, S. K. Farrand, Quorum sensing but not autoinduction of Ti plasmid conjugal transfer requires control by the opine regulon and the antiactivator TraM. *J. Bacteriol.* **182**, 1080–1088 (2000).
24. M. J. Gambello, B. H. Iglewski, Cloning and characterization of the *Pseudomonas aeruginosa lasR* gene, a transcriptional activator of elastase expression. *J. Bacteriol.* **173**, 3000–3009 (1991).
25. J. H. Lee, Y. Lequette, E. P. Greenberg, Activity of purified QscR, a *Pseudomonas aeruginosa* orphan quorum-sensing transcription factor. *Mol. Microbiol.* **59**, 602–609 (2006).
26. J. Lee, L. Zhang, The hierarchy quorum sensing network in *Pseudomonas aeruginosa*. *Protein Cell* **6**, 26–41 (2015).
27. M. Schuster, M. L. Urbanowski, E. P. Greenberg, Promoter specificity in *Pseudomonas aeruginosa* quorum sensing revealed by DNA binding of purified LasR. *Proc. Natl. Acad. Sci. U.S.A.* **101**, 15833–15839 (2004).
28. M. Schuster, C. P. Lostroh, T. Ogi, E. P. Greenberg, Identification, timing, and signal specificity of *Pseudomonas aeruginosa* quorum-controlled genes: A transcriptome analysis. *J. Bacteriol.* **185**, 2066–2079 (2003).
29. T. de Kievit, P. C. Seed, J. Nezezon, L. Passador, B. H. Iglewski, RsaL, a novel repressor of virulence gene expression in *Pseudomonas aeruginosa*. *J. Bacteriol.* **181**, 2175–2184 (1999).
30. L. Passador, J. M. Cook, M. J. Gambello, L. Rust, B. H. Iglewski, Expression of *Pseudomonas aeruginosa* virulence genes requires cell-to-cell communication. *Science* **260**, 1127–1130 (1993).
31. B. J. Burkinshaw *et al.*, A type VI secretion system effector delivery mechanism dependent on PAAR and a chaperone-co-chaperone complex. *Nat. Microbiol.* **3**, 632–640 (2018).
32. J. D. Dockery, J. P. Keener, A mathematical model for quorum sensing in *Pseudomonas aeruginosa*. *Bull. Math. Biol.* **63**, 95–116 (2001).
33. M. H. J. Sturme *et al.*, Cell to cell communication by autoinducing peptides in gram-positive bacteria. *Antonie van Leeuwenhoek* **81**, 233–243 (2002).
34. B. A. Hense *et al.*, Does efficiency sensing unify diffusion and quorum sensing? *Nat. Rev. Microbiol.* **5**, 230–239 (2007).
35. G. Rampioni *et al.*, The quorum-sensing negative regulator RsaL of *Pseudomonas aeruginosa* binds to the *lasI* promoter. *J. Bacteriol.* **188**, 815–819 (2006).
36. V. Bettenworth *et al.*, Phenotypic heterogeneity in bacterial quorum sensing systems. *J. Mol. Biol.* **431**, 4530–4546 (2019).
37. C. Anetzberger, T. Pirch, K. Jung, Heterogeneity in quorum sensing-regulated bioluminescence of *Vibrio harveyi*. *Mol. Microbiol.* **73**, 267–277 (2009).
38. J. Grote *et al.*, Evidence of autoinducer-dependent and -independent heterogeneous gene expression in *Sinorhizobium fredii* NGR234. *Appl. Environ. Microbiol.* **80**, 5572–5582 (2014).
39. P. D. Pérez, S. J. Hagen, Heterogeneous response to a quorum-sensing signal in the luminescence of individual *Vibrio fischeri*. *PLoS One* **5**, e15473 (2010).
40. J. W. Williams, X. Cui, A. Levchenko, A. M. Stevens, Robust and sensitive control of a quorum-sensing circuit by two interlocked feedback loops. *Mol. Syst. Biol.* **4**, 234 (2008).
41. M. Ackermann, A functional perspective on phenotypic heterogeneity in microorganisms. *Nat. Rev. Microbiol.* **13**, 497–508 (2015).
42. C. J. Davidson, M. G. Surette, Individuality in bacteria. *Annu. Rev. Genet.* **42**, 253–268 (2008).
43. C. van Delden, R. Comte, A. M. Bally, Stringent response activates quorum sensing and modulates cell density-dependent gene expression in *Pseudomonas aeruginosa*. *J. Bacteriol.* **183**, 5376–5384 (2001).
44. R. Gupta, M. Schuster, Negative regulation of bacterial quorum sensing tunes public goods cooperation. *ISME J.* **7**, 2159–2168 (2013).
45. B. E. Eaton, L. Gold, D. A. Zichi, Let's get specific: The relationship between specificity and affinity. *Chem. Biol.* **2**, 633–638 (1995).
46. Y. Chai, J. Zhu, S. C. Winans, TrlR, a defective TraR-like protein of *Agrobacterium tumefaciens*, blocks TraR function in vitro by forming inactive TrlR:TraR dimers. *Mol. Microbiol.* **40**, 414–421 (2001).
47. C. Wang, C. Yan, C. Fuqua, L. H. Zhang, Identification and characterization of a second quorum-sensing system in *Agrobacterium tumefaciens* A6. *J. Bacteriol.* **196**, 1403–1411 (2014).
48. I. S. Barton *et al.*, Co-dependent and interdigitated: Dual quorum sensing systems regulate conjugative transfer of the Ti plasmid and the At megaplasmid in *Agrobacterium tumefaciens* 15955. *Front. Microbiol.* **11**, 605896 (2021).
49. B. W. Holloway, V. Krishnapillai, A. F. Morgan, Chromosomal genetics of *Pseudomonas*. *Microbiol. Rev.* **43**, 73–102 (1979).
50. W. G. Miller, J. H. Leveau, S. E. Lindow, Improved *gfp* and *inaZ* broad-host-range promoter-probe vectors. *Mol. Plant Microbe Interact.* **13**, 1243–1250 (2000).
51. R. Wilton *et al.*, A new suite of plasmid vectors for fluorescence-based imaging of root colonizing pseudomonads. *Front. Plant Sci.* **8**, 2242 (2018).
52. M. Jahn, C. Vorpahl, T. Hübschmann, H. Harms, S. Müller, Copy number variability of expression plasmids determined by cell sorting and droplet digital PCR. *Microb. Cell Fact.* **15**, 211 (2016).
53. B. B. Pradhan, S. Chatterjee, Reversible non-genetic phenotypic heterogeneity in bacterial quorum sensing. *Mol. Microbiol.* **92**, 557–569 (2014).
54. R. Chuanchuen, C. T. Narasaki, H. P. Schweizer, Benchtop and microcentrifuge preparation of *Pseudomonas aeruginosa* competent cells. *Biotechniques* **33**, 760–763, 762–763 (2002).
55. C. N. Wilder, S. P. Diggle, M. Schuster, Cooperation and cheating in *Pseudomonas aeruginosa*: The roles of the *las*, *rhl* and *pqs* quorum-sensing systems. *ISME J.* **5**, 1332–1343 (2011).
56. T. T. Hoang, R. R. Karkhoff-Schweizer, A. J. Kutchma, H. P. Schweizer, A broad-host-range Flp-FRT recombination system for site-specific excision of chromosomally-located DNA sequences: Application for isolation of unmarked *Pseudomonas aeruginosa* mutants. *Gene* **212**, 77–86 (1998).